

THERMOACOUSTIC RANGE VERIFICATION FOR ION THERAPY

S.K. Patch^{1*}, Y.M. Qadadha, UW-Milwaukee, Milwaukee WI 53211
 M. Kireeff-Covo^{2*}, A. Jackson, K.S. Campbell, R.A. Albright, P. Bloemhard, A.P. Donoghue,
 C.R. Siero, T.L. Gimpel, S.M. Small, B.F. Ninemire, M.B. Johnson, and L. Phair
 Lawrence Berkeley National Laboratory, Berkeley CA 94720
 * corresponding authors for ^{1*}thermoacoustics and ^{2*}chopper engineering

Abstract

The clinical value of particle therapy is limited by inaccurate range verification, currently assumed to be 1 mm + 3.5% of the target depth. The purpose of this work was to correlate the Bragg peak location with target morphology, by overlaying the location of the Bragg peak onto a standard ultrasound image. A fast chopper installed between the ion source and the cyclotron inflector pulsed delivery of 50 MeV protons so that 4 pC were delivered in 2 μ s, depositing 2 Gy in the Bragg peak. The ion pulse generated thermoacoustic pulses that were detected by a cardiac ultrasound array, which also produced a grayscale ultrasound image. A filtered backprojection algorithm focused the received signal to the Bragg peak location with perfect co-registration to the ultrasound images. Data was collected in a room temperature water bath and gelatin phantom with a cavity designed to mimic the intestine, in which gas pockets can displace the Bragg peak. Thermoacoustic range measurements agreed with Monte Carlo simulation and first-order range estimates from CT images to within 1.5 mm.

MOTIVATION/INTRODUCTION

Proton therapy delivers less dose to proximal tissue, and spares distal tissue altogether. Evidence-based medicine currently supports the use of proton therapy only for tumors near the base of the neck, spine, eye and in pediatric patients [1]. Lack of accurate range verification otherwise limits clinical utility of proton therapy [2]. Short-lived positron [3] and prompt gamma emissions [4, 5] can provide fast and real-time feedback, respectively, but do not correlate the Bragg peak location with anatomy. An automated method for correlating PET data to underlying anatomy in CT images [6] is slow and precludes online adaptive planning.

Thermoacoustic range verification is a natural consequence of the conversion of deposited dose to mechanical pressure pulses. Treatment plans are quantified in terms of Grays, 1 Gy = 1 J/kg [7], whereas acoustic pulse amplitudes are quantified by Pascals, 1 Pa = 1 N/m² = 1 J/m³. The units for dose and pressure differ only by a multiplicative factor of target density, ρ . The dimensionless Grüneisen (Γ) is simply the constant of proportionality between energy density and thermally induced pressure change. In soft tissue, $\Gamma \sim 0.1$, so the rule of thumb is that 100 Pa are generated per Gy, provided stress confinement holds and the deposition rate exceeds the rate at which pressure propagates away from the

target. Fig. 1 models pressures generated by single turn delivery of a 2 Gy dose due to a 49 MeV beam.



Figure 1: Pressure and dose in waterbath due to 49 MeV beam. Dose in Gy plotted in yellow, overlaid on a cross-sectional image of pressure due to single turn extraction. Distal transducer location indicated by yellow square.

Regardless of spill time, thermoacoustic pulses measured at distant transducer locations are diminished by several factors. $1/r$ geometric spreading is unavoidable. Fortunately, acoustic absorption and scatter are less significant in the very low frequency regime of thermoacoustic emissions. Thermoacoustic emissions generated by instantaneous, “single turn” delivery of 4 pC are compared to those generated by spill times of 2, 6 and 18 μ s in Fig. 2.

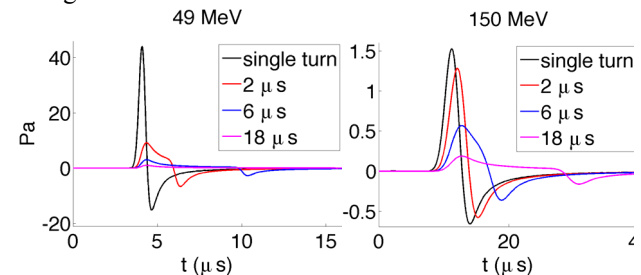


Figure 2: Thermoacoustic measurements at distal transducer locations as a function of spill time. 49 MeV (left) and 150 MeV (right) beams with transducer 6.5 mm and 20 mm distal, respectively.

Long spill times allow pressure to propagate away as ions continue to be deposited. Transit time across the Bragg peak of a 49 MeV beam is less than a 2 μ s spill time, which diminishes measured pressures four-fold, as seen by the red plot in Fig. 2 (left). Straggling broadens the Bragg peak of a 150 MeV beam, increases acoustic transit time so that a 2 μ s spill preserves amplitude, whereas a 6 μ s spill does not as shown in Fig. 2 (right).

Experimentally, 2 μ A of 50 MeV protons were delivered for 2 μ s. An injection line chopper (Fig. 3) limited the energy deposited by low energy beams, delivering 2 Gy in a single pulse. Unlike previous results in which thermoacoustic emissions were detected by single-element transducers or hydrophones without online correlation to anatomy, and recently two different ultrasound arrays were used to receive thermoacoustic emissions and generate ultrasound images of a mouse leg [8]. We used the

same clinical ultrasound array to acquire thermoacoustic signal and generate ultrasound images, ensuring perfect coregistration of range estimates with underlying morphology [9].

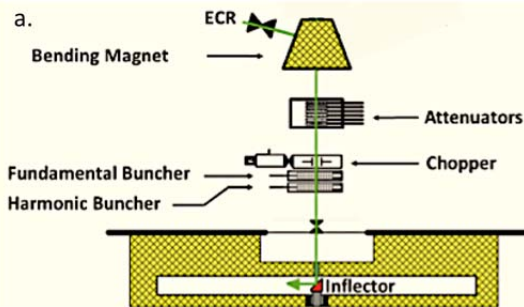


Figure 3: Axial injection line, including fast chopper and electron cyclotron resonance (ECR) ion source.

METHODS AND MATERIALS

The experiment was conducted at the 88" Cyclotron at Lawrence Berkeley National Laboratory, which is a sector-focused cyclotron with energy constant K of 140. The cyclotron was tuned to produce 50 MeV protons, which lost approximately 1 MeV in an ion chamber before entering the target. Thermoacoustic emissions were collected during a 28-hour shift. A clinical ultrasound transducer array detected thermoacoustic emissions from locations on the beamline distal to the Bragg peak.

Beamline and Chopper

An injection line chopper deflected the beam as it passed between parallel plates, allowing protons to pass to the cyclotron only when the plates were discharged. There is no dosimetric consequence by deflecting the beam at the injection line, before it is accelerated by the cyclotron, because the beam is at low energy, i.e., less than 25 keV/u.

The chopper uses a fast square wave pulser (Behlke, model FSWP-51-02) that can provide ± 1 kV and is connected to two parallel electrostatic deflector plates, which are 6" wide and 3.25" long with a separation of 3.25". Results below were generated by a pulsewidth on the injection line of 1.5 μ s. Proton pulses were delivered at a repetition frequency of 100 Hz.

The pulsers are formed by series-connected power metal oxide semiconductor field-effect transistors (MOSFETs), which are triggered synchronously by a galvanically isolated driver control circuit. The unit has a floating configuration, so it can produce positive or negative pulses by grounding the positive or negative end of the push-pull arrangement. To match the impedance and to protect the switches, series resistors are built in. Internal ceramic capacitors ensure adequate buffering of the external high voltage supply. The pulser has direct liquid cooling that uses a dielectric liquid with excellent specific heat capacity and insulation, so it can continuously switch at 3 MHz with a maximum power dissipation of 1500 W. The pulser is protected against overheating due to rapid frequency switching by a thermal interlock that disables the control circuit when the temperature exceeds 75 °C.

Ultrasound Hardware and Data Processing

Thermoacoustic emissions were measured by a programmable ultrasound system (Verasonics V1) with a 96-channel P4-1 cardiac array (ATL), as described in [9]. 1024 proton pulses were averaged to visualize the Bragg peak in the data as displayed in real-time on a computer monitor.

Targets

Two targets were utilized. A water bath provided a homogeneous and characterizable target with low acoustic attenuation. A gelatin phantom with nominal soft tissue properties ultrasonic properties [10] was fabricated with a cavity to mimic the intestine. Range estimation was performed with the intestinal cavity both empty and full of olive oil to demonstrate feasibility of detecting anatomic change due to digestion.

RESULTS

Water Tank Results

The pulse emanating from the Bragg peak was nearly spherical, and travelled outward in all directions. The part that travelled towards the entrance wall was reflected and returned to the transducer array. All three pulses, Bragg peak direct, LDPE direct and Bragg peak reflected, can be seen in Fig. 4a-c, where readouts from all 96 transducer channels are displayed.

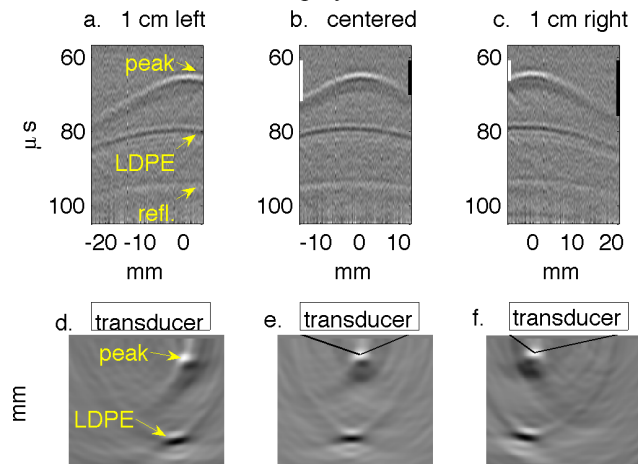


Figure 4: Water tank results in which transducer is translated in 1 cm increments perpendicular to the beamline. The transducer axis is 1 cm left, centered and 1 cm right of the beamline in Figs. a & d, b & e, and c & f, respectively. (a-c) Filtered P4-1 data with timing measured from chopper plate discharge, not entry of beam into target. Horizontal axes represent channel number. (d-f) Reconstructions of the data reveal the Bragg peak as a monopole 6.5 mm from the transducer. The proximal end of the beam as it enters the LDPE appears as a bipolar mark.

Because the transducer's 2.8 cm lateral width exceeded its axial distance from the Bragg peak by a factor of four, channels on the array closest to the Bragg peak detected signal sooner than those on either end, causing arc-shaped first arrivals in the data show in Figs. 4 a-c.

White and black vertical lines in Figs. 4 b-c represent delays between proton delivery and first arrival of the Bragg peak signal in channels 1 and 96 on either end of the transducer array. White and black lines in reconstructed images in Figs. 4 e-f have length of the corresponding time delays multiplied by soundspeed.

The P4-1 array was positioned about 1" from tank wall, attached to a stepper motor that translated nearly parallel to vertical tank wall. Data was collected at three transducer positions: centered with respect to the Bragg peak, and translated right and left by 1 cm each. Shifted arcs in filtered data shown in Figs. 4 a-c correspond to shifted Bragg peak locations reconstructed in Figs. 4 d-f.

Phantom Results

Images in Fig. 5 show translation of the Bragg peak due to air in the intestinal cavity and highlight the difficulty of using ultrasound imaging alone for range verification. Filtered time series and reconstructed thermoacoustic images are shown above grayscale ultrasound images with overlays of Bragg peak location in yellow and beam entry point in red. Sagittal images with the cavity filled with olive oil and empty are shown in the "a" and "b" subfigures, respectively. The oil-filled cavity in Fig. 5a appears as an anechoic dark region, but reflection of ultrasound at an air/tissue interface in Fig. 5b makes the speckle pattern inside the cavity similar to that of the surrounding phantom material.

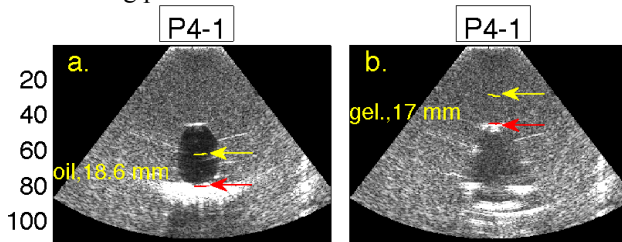


Figure 5: Overlays onto grayscale ultrasound images. Subfigures are labelled with letters corresponding to transducer orientation and cavity status. (a) Cavity filled with olive oil. (b) Cavity empty. Grayscale ultrasound image with Bragg peak overlaid in yellow; beam entry point into high stopping power target in red.

Range in the phantom was estimated from CT scans as detailed in [9]. Overlays of the Bragg peak onto the gelatin phantom agree within 1.4 mm, but overestimate the range in non-aerated olive oil by 1.1 mm.

DISCUSSION

We have presented two synergistic and novel improvements to thermoacoustic range verification: First, proton pulses delivered a therapeutic dose of 2 Gy in less than $2 \mu\text{s}$, and generated broadband thermoacoustic emissions. Second, a clinical ultrasound array detected those pulses to create images of the Bragg peak that are perfectly co-registered with ultrasound images that can display the treatment field.

The importance of short spill times decreases with proton energy. At high energies, straggle spreads beam

and reduces requirements on chopper – but also reduces sharpness of Bragg peak and makes range verification more difficult.

Similar choppers can be installed in any system with sufficient space for a deflector plate between the ion source and the point at which the beam is accelerated, *i.e.* before the cyclotron inflector for external ion sources or close to the cyclotron middle region for internal ion sources.

CONCLUSION

Thermoacoustic range verification with better than 1.5 mm accuracy in homogeneous targets has been demonstrated with a commercial clinical ultrasound array, but at doses exceeding the clinical realm. Further optimization of both transducer array and fast delivery of an intense beam will be required to enable online adaptive planning for treating tumors that can be visualized by ultrasound.

ACKNOWLEDGMENT

We thank M. Zolotorev and the late A. Sessler for introducing us to thermoacoustic range verification. This work was supported in part by the Director, Office of Science, Office of Nuclear Physics, of the U.S. Department of Energy under Contract No. DE-AC02-05CH11231.

REFERENCES

- [1] "American Society for Therapeutic Radiology and Oncology - Model Policies, Proton Beam Therapy (PBT)," in *Indications and Limitations of Coverage and/or Medical Necessity - Group 2*, ed, 2013.
- [2] A. C. Knopf and A. Lomax, "In vivo proton range verification: a review," *Phys Med Biol*, vol. 58, pp. R131-60, Aug 7 2013.
- [3] P. Dendooven *et al.*, "Short-lived positron emitters in beam-on PET imaging during proton therapy," *Phys Med Biol*, vol. 60, pp. 8923-47, Dec 7 2015.
- [4] F. Hueso-Gonzalez *et al.*, "First test of the prompt gamma ray timing method with heterogeneous targets at a clinical proton therapy facility," *Phys Med Biol*, vol. 60, pp. 6247-72, Aug 21 2015.
- [5] C.-H. Min *et al.*, "Prompt gamma measurements for locating the dose falloff region in the proton therapy," *Applied Physics Letters*, vol. 89, p. 183517, 2006.
- [6] K. Frey *et al.*, "Automation and uncertainty analysis of a method for in-vivo range verification in particle therapy," *Phys Med Biol*, vol. 59, pp. 5903-19, Oct 7 2014.
- [7] J. Selman, *The Fundamentals of Imaging Physics and Radiobiology*, Charles C Thomas, 2000.
- [8] S. Kellnberger *et al.*, "Ionoacoustic tomography of the proton Bragg peak in combination with ultrasound and optoacoustic imaging," *Scientific Reports*, vol. 6, p. 29305, 2016.
- [9] S. Patch *et al.*, "Thermoacoustic Range Verification using a Clinical Ultrasound Array Provides Perfectly co-Registered Overlay of the Bragg peak onto an Ultrasound Image," *Physics in Medicine and Biology*, vol. 61, pp. 5621-5638, 2016.
- [10] M. Lazebnik *et al.*, "Tissue-mimicking phantom materials for narrowband and ultrawideband microwave applications," *Physics in Medicine and Biology*, vol. 50, pp. 4245-4528, 2005.